Reconfigurable Optical Boolean Function Generator Based on Electro-Optical Nonlinear Dynamics

Xingxing Jiang, Mengfan Cheng,* Yudi Fu, Chenkun Luo, Quan Yu, Linbojie Huang, Fengguang Luo, Lei Deng, Minming Zhang, and Deming Liu

Next Generation Internet Access National Engineering Lab (NGIA-NEL), School of Optical and Electronic Information, Huazhong University of Science and Technology (HUST), Wuhan 430074, China

(Received 25 September 2019; revised manuscript received 20 February 2020; accepted 18 March 2020; published 9 April 2020)

We propose an optical Boolean function generator based on an electro-optical nonlinear feedback loop. Theoretically, all possible Boolean functions with optical input and output can be implemented by passing through enough iterations. By changing the control signal, the optical circuit can be configured to any desired Boolean function without adjusting the physical setup. Optical components with high bandwidth can improve the computing speed markedly. The impact of noise on the system is considered in detail. The results show that a substantial number of reliable Boolean functions can be obtained in the presence of noise contamination. Compared with traditional optical digital computation systems, the proposed scheme exhibits a huge advantage in multifunctional computing and flexible configuration.

DOI: 10.1103/PhysRevApplied.13.044025

I. INTRODUCTION

Traditional electric computation seems to be squeezing out its potential with the failure declaration of Moore's law [1,2]. As the requirement of data processing rapidly grows, electrical computation might be confronted with challenges in the future. Optics, with the nature of broad band and parallel processing, has gained considerable attention in various aspects [3–5]. Therefore, increasing interest is given to seeking an alternative computation system realized by the optical method [6–8]. Numerous scenarios based on an optical mechanism have been put forward in recent years.

Most of these optical schemes can be cataloged into two main groups, namely digital computation and analog computation. Following the development track of electrical digital computers, various implementations of optical transistors and optical logic gates are investigated. Among these, making use of optical nonlinear effects to implement an optical transistor is a popular issue. In Ref. [9], the direct control of a strong optical signal by a weak optical signal was proved to be feasible in optical material. Taking advantage of the nonlinear effect in optical fiber, the idea that combines optical logical operation and communication has aroused the interest of some researchers [10]. A semiconductor optical amplifier, as a potential candidate for optical gates, is attractive in optical computations [11–14]. By fully exploiting its inherent cross-phase modulation, cross-gain modulation, and four-wave mixing, several fundamental logical gates can be acquired. However, through these methods, only few simplistic combinatorial logic functions or finite-state machines can be accomplished. Moreover, to perform a different logic operation, a physical reconfiguration is usually required. This can harness the complexity of implementing an optical computation system.

Using optical analog systems to execute some specific calculation tasks is another method leading to optical computation. Optical lens organized to acquire the fractional Fourier transform or others have been widely investigated on the basis of a $4f$ system [15,16]. Combining a phase modulator (PM) and dispersive media, an identical function can be attained in an optical fiber system [17]. Recently, a further study revealed a scheme of an optical time-domain stretcher, which is constructed by a similar setup [18]. Besides various optical transformations, the physical implementations of a neural network by virtue of optical systems have attracted growing interest. Based on the time-delay optical chaotic structure, the concept of reservoir computing is proposed, which can be used to improve the transmission performance of optical fiber communication [19–23]. Reference [24] demonstrated a fully optical scheme to implement general deep neural-network algorithms by cascading Mach-Zehnder interferometers in a silicon integrated circuit. However, under the effect of accumulated noise in cascaded stages or feedback, the practical application of analog optical computation still faces big challenges [10]. In brief, studies on optical computation, whether using analog or digital methods, have many problems to solve yet.

*chengmf@mail.hust.edu.cn

 © 2020 American Physical Society

Recently, Kia *et al.* provide another view to elevate the computing ability of electrical nonlinear systems [25,26]. Utilizing the ergodicity, nonperiod, and initial-value sensitivity properties [27–29], an electrical chaos system can generate a tremendous number of Boolean functions through mapping the Boolean input and control bit onto an initial value. Since different control signals project the input bits onto different initial states, outputting various Boolean functions can be possible through amplifying the difference of initial values under the participation of nonlinear chaotic iterations. Nevertheless, there might be some challenges when it is extended to realize a faster calculation task. Firstly, most of the electrical nonlinear components operate at a relatively low-frequency range, which can not deal with the requirement of robust fast computing. Secondly, a fast precise mapping from multiple input bits to analog values is needed. In Ref. [25], this process is performed by a high-resolution DAC. However, a DAC with both high operation frequency and high resolution is always costly and difficult to implement. Moreover, chaos circuits are super sensitive to initial values, which imposes a restriction requirement on the accuracy and stability of mapping. The DAC is replaced by an averaging circuit in Ref. [26], but a combinational logic circuit composed of electrical XOR gates is used, which might affect its performance.

An optical scheme is usually used as a solution for applications with the requirement for high-speed signal operation. Therefore, establishing this computing scheme in optical field is an attractive idea. It is stated that any desired complex optical waveform can be performed by time-domain multiplane light-conversion technology, which consists of a recirculating loop, including a PM and a fiber Bragg grating (FBG) [30]. The output waveform is determined by the detailed driving signal of a PM. Meanwhile, optical chaotic systems based on a PM and FBG can exhibit complex dynamic properties [31,32]. Inspired from these phenomena, it might be a promising supposition to implement a controllable optical Boolean function generator by PM and FBG structure.

In this paper, we propose a reconfigurable optical Boolean function generator based on an optical nonlinear iteration loop. Due to the intrinsic broadband properties of photonic devices, a high-speed output can be obtained. Different from the electrical methods, a serial waveform is adopted as the input. Thus, the requirement of precise input coding can be avoided. The desired Boolean function is selected by changing the form of nonlinear iteration, which is directly determined by the serial control bits. Through choosing the corresponding control signal, the Boolean function can be rewritten as expected. After adequate nonlinear iterations, finally all possible multi-input Boolean functions can be achieved in a system without changing the physical configuration.

II. PRINCIPLE

Considering an N-bit input one-bit output Boolean function, there are 2^N combinations of input data when each input only takes binary value. The total number of attainable Boolean functions is 2^{2^N} as a different one can be acquired through reversing its output state. For instance, two binary inputs can combine four conditions: (0, 0), (0, 1), (1, 0), and (1, 1). The output can be 0 or 1 for each input combination. Hence, 2^{2^2} distinct Boolean functions exist in theory.

As depicted in Fig. 1(a), a nonlinear feedback circuit under external control is designed as the generator to obtain a reconfigurable Boolean function. Accordingly, the information flow needs to go through three stages, namely coding, nonlinear iteration, and decoding. In the coding process, the paralleled Boolean input is converted into N-bit serial sequence. Then the sequence is sent to the optical nonlinear circuit as the initial state of iteration. If $g(.)$ denotes the transformation of nonlinear iteration, this process can be described by Eqs. (1) and (2):

$$\text{output}(l) = g[\text{input}(l-1), \text{control}(C_0, C_1, \ldots, C_{2^N-1})], \quad l = 1, 2, 3, \ldots, \tag{1}$$

$$\text{input}(l) = \text{output}(l), \tag{2}$$

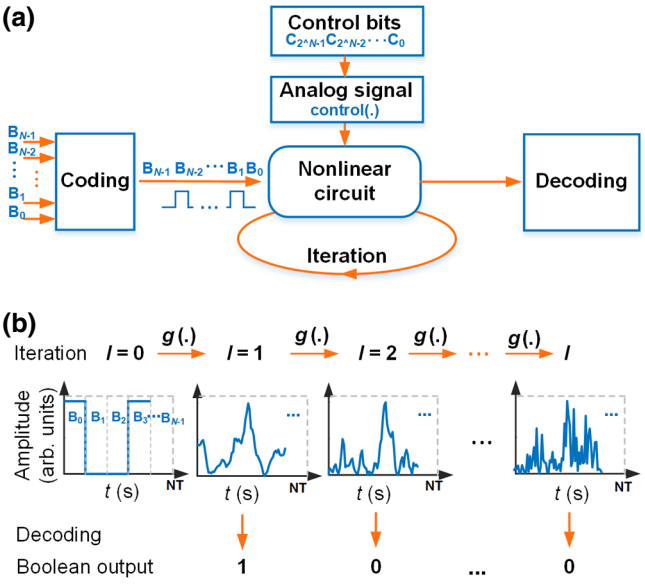

FIG. 1. (a) is the fundamental frame of proposed optical Boolean function generator; (b) shows a typical illustration for iteration process. The nonlinear function $g(.)$ treats the whole segment of waveform with duration of NT as input. Here, N denotes the number of input Boolean bits and T represents the duration time of unit pulse. After the delay induced by feedback ciruit, the output of $g(.)$ will be the input for the next iteration.

where l represents the number of iteration times. control(.) represents a gallery containing 2^{2^N} different analog control signals, which is selected by setting different control bits $C_0, C_1, \ldots C_{2^N-1}$. input($l$) is the optical incident signal at the lth iterating, input(0) denotes the serially injected optical Boolean input. output(l) is the output signal at the lth iteration. The output of the current iteration is the input signal in the next cycle. The obtained equations are similar to the discrete chaotic iteration equations, where a segment of waveform instead of a single value is used as the initial input. Figure 1(b) shows an example illustrating the iteration process.

A segment of analog waveform determined by the binary control bits is served as the control signal of the nonlinear circuit. In other words, the control bits influence the system output through changing nonlinear transformation $g(.)$. For specific control data, the control signal remains the same in each iteration. Finally, a decoder is used to transform a segment of output waveform to a Boolean value.

Compared with the electrical methods, a serial waveform, rather than a precise initial state, is used as the input. Therefore, the accurate mapping procedure is not in need. In order to distinguish the achievable Boolean functions, a control signal of 2^{2^N} different states is required. Control signal is used as an independent driving source of nonlinear iteration. By changing control signal, a different nonlinear function is applied to the input signal as indicated in Eq. (1). Different from electrical methods, a control data matches a Boolean function through varying nonlinear iteration equation. Theoretically, the mapping between analog driving waveform and control bits can be arbitrarily chosen. Therefore, a flexible configuration of control signal can be adopted according to the occasions. Under the fast response frequency of optical devices, high-speed computing can be achieved.

III. SYSTEM SETUP

Based on the principle above, a typical structure of the proposed scheme is depicted in Fig. 2. The optical Boolean input is obtained through modulating the light emitted from the directly modulated laser (DML) by input bits with bitrate f. An acoustic-optic modulator (AOM1) is applied to turn off the direct current light from the laser after the initial stage. The mathematical model of this process can be simply expressed by the following equations:

$$E_{\text{init}}(t) = A(t)\exp(j\omega_0 t + \phi_0), \tag{3}$$

$$A(t) = \begin{cases} aB_n, & nT \le t < (n+1)T \\ 0, & \text{otherwise} \end{cases}, \tag{4}$$

where E_{init} is the output optical signal, ω_0 denotes the frequency of DML and ϕ_0 is the constant phase shift.

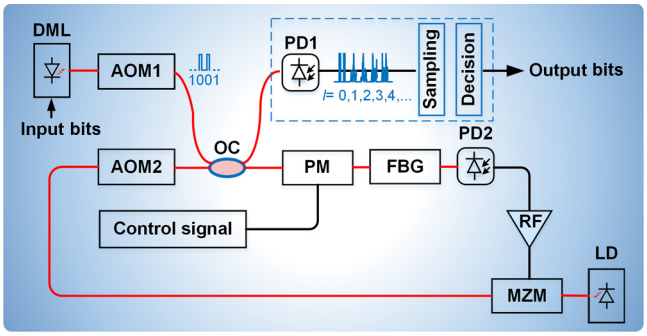

FIG. 2. System setup of proposed optical Boolean function generator. DML, directly modulated laser; AOM, acoustic-optic modulator; OC, optical coupler; PM, phase modulator; FBG, fiber Bragg grating; PD, photodetector; MZM, Mach-Zehnder modulator; rf, radiofrequency amplifier; LD, laser diode.

$A(t)$ is the modulation signal with amplitude a, which is determined by input bits $\{B_n\}$, where $n = 0, 1, \ldots N-1$. T represents the duration times of unite pulse, equaling $1/f$.

Then the generated optical signal is injected into the nonlinear feedback loop through a 50:50 optical coupler (OC). The feedback loop is made up of two parts, the first including a PM, an FBG, a photodetector (PD2) and the other mainly consisting of a Mach-Zehnder modulator (MZM). After once transmission from PM to MZM, one nonlinear transformation completes. The first iteration starts after the injection of $E_{\text{init}}(t)$. PM receives this segment of optical signal and adds the control signal on its phase. Passing through the whole loop, a portion power of this segment of optical signal is coupled to the decoder, then outputting the result of the first iteration. The other is used as the input in the next iteration. Through the PM, this segment of sequence is phase modulated by the same control signal continuously during iterations. The control signal x is generated by control bits and used to drive the electrical port of PM. AOM2 is inserted in the feedback circuit to determine the loop on-off. By properly setting its modulating signal, precise control of loop iteration times can be established. The output optical field $E_2(t)$ can be given by

$$E_2(t) = E_1(t)\exp\left\{j\pi m_1 x\left[\text{ceil}\left(\frac{t-l\tau}{T}\right)\right]\right\}, \quad l\tau < t \le l\tau + NT, \tag{5}$$

$$E_1(t) = E_{\text{init}}(t) + E_{\text{feed}}(t). \tag{6}$$

Here, ceil(.) denotes the nearest integer larger than or equal to the variable, m_1 is the modulation depth of PM, l indexes the current iteration time, and NT represents the duration of the optical Boolean input $E_{\text{init}}(t)$. τ is the delay time of

the whole feedback loop, which should be larger than NT to ensure the independence of each iteration. $E_1(t)$ denotes the optical field of incident light of the PM, which is equal to $E_{\text{init}}(t)$ at the initial step ($l = 0$) but replaced by the feedback light $E_{\text{feed}}(t)$ at the beginning of iterations ($l \geq 1$). Under the same control condition, E_{feed} is phase modulated by the same segment of control signal x.

After phase modulation, the obtained optical signal is then sent into a dispersive media, which is performed by a FBG. The FBG is used to implement the phase modulation to intensity modulation conversion of the phase-modulated carrier [33], where its transfer function in the frequency domain is described as

$$H(\omega) = \exp\left[j\frac{d}{2}(\omega - \omega_0)^2\right], \tag{7}$$

where d denotes the dispersion value.

The output optical field of FBG can be written as $E_3 = E_2(t) \circ h(t)$, where "$\circ$" denotes the convolution operation and $h(t)$ corresponds to the time-domain expression of $H(\omega)$. Sequentially, the optical signal is captured by a photodetector (PD2). The output electrical signal can be expressed by

$$x_2 = \left|[E_2(t) \circ h(t)] \times [E_2(t) \circ h(t)]^*\right|, \tag{8}$$

where "$*$" denotes the complex conjugate operator. PM, FBG, and PD2 form an optical transform, through which the control signal is mixed with the input waveform and participates in the iteration process.

The detected signal x_2 is amplified and modulated onto another light wave with an MZM, which completes the optical feedback loop. The process can be expressed by

$$E_{\text{feed}}(t) = \sqrt{P}\cos[\pi m_2 x_2(t) + \phi_{\text{bias}}]\exp(j\omega_1 t + \phi_1), \tag{9}$$

$$m_2 = \frac{\gamma\alpha}{V_{\text{pi}}}. \tag{10}$$

P is the average power of the light generated from laser diode (LD), ω_1 is the angular frequency, and ϕ_1 is the initial phase of optical carrier. m_2 describes the modulation depth of MZM. γ and α represent the responsivity of PD2 and the gain induced by rf amplifier, respectively. V_{pi} denotes the half-wave voltage of the MZM and ϕ_{bias} is the bias phase. The electric input of MZM is amplified by the rf, which means that the amplitude of the input can span one or several V_{pi} of the modulator's transfer function. Therefore, MZM is working in its nonlinear region and can be seen as a nonlinear noninvertible transformation [34]. Through adjusting the modulation depth of MZM, the degree of nonlinearity can be freely adjusted. After numerous iterations, this optical nonlinear feedback loop can exhibit chaotic behavior and generate infinite states in theory.

The last part of the system is the decoder. The resulted optical signal $E_o(t)$ split from OC is converted into electrical signal x_3 by PD1. Then x_3 is delivered to the decoder, which consists of a sampling module and a decision circuit. The decoding process can be described by

$$x_o(l) = x_3\left(l\tau + \frac{NT}{2}\right), \tag{11}$$

$$o(l) = \begin{cases} 0, & x_o(l) \leq x_{\text{th}} \\ 1, & x_o(l) > x_{\text{th}} \end{cases}. \tag{12}$$

$x_o(l)$ indicates the obtained real value after sampling at the lth iteration. By comparing with the threshold value of the decision circuit x_{th}, the state space is partitioned into two parts. Finally, a Boolean state $o(l)$ outputs.

The whole system can be cataloged into three parts according to the principle. DML is used to convert electric logical input into an optical waveform, performing the coding function. The decoding process is implemented through a PD and one-bit comparator circuit. The nonlinear iteration contains a two-level optical transform, where the first level corresponds to Eqs. (5)–(8) and the second level corresponds to Eqs. (9) and (10). Control signal, as an independent driving source, determines the detailed nonlinear transform applied on the Boolean input. In our scheme, multilevel control waveform x is produced from the binary control bits. In order to generate 2^{2^N} segments of different control waveforms with 2^N control bits, we define the format of the control waveform firstly. Here, one segment of control waveform is composed of N pulses, which can be denoted by $\{x(0), x(1),\ldots, x(N-1)\}$. Then constructing an $M \times N$ matrix, the 2^N control bits are filled into the matrix, and the values of the remaining elements are assigned as constant 0 or 1. M is calculated as Eq. (13) to make sure that $M \times N \geq 2^N$. If S_m represents the element from the matrix, the projection process can be described by Eq. (14). Then, M elements in each column of the matrix are mapped onto one pulse, and the mapping rule is defined by Eq. (15). Equation (15) means that the weights of the M elements are different. As a result, there could be 2^M possible states for each pulse $x(n)$, which form a multilevel waveform. According to Eqs. (13) and (14), there are 2^{2^N} different possible shapes for the whole control waveform. Thus, 2^N control bits are rearranged to N pulses, and 2^{2^N} states of the control signal are obtained.

$$M = \text{ceil}(2^N/N), \tag{13}$$

$$S_m = \begin{cases} C_m, m < 2^N \\ 0, m \geq 2^N \end{cases}, \tag{14}$$

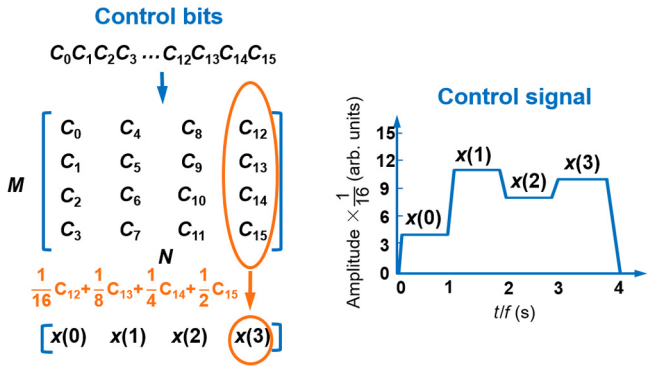

FIG. 3. Generation of control signal from control bits for 4-bit Boolean input.

$$x(n) = \sum_{m=nM}^{(n+1)M-1} 2^{m-(n+1)M} S_m, n = 0, 1, 2, \ldots, N-1. \tag{15}$$

To illustrate this scheme more clearly, we use a 4-bit input Boolean function as an example, namely $N = 4$. As shown in Fig. 3, its 16 control bits are rearranged to a 4×4 matrix. After the weighting and superposition operation according to Eq. (15), which can be established by conventional proportional amplifier and adder circuit, each column in the matrix corresponds to a pulse with 2^M $(= 16)$ discrete amplitudes. Finally, $16^N = 65\,536$ different control waveforms can be obtained by assigning the values of 16 control bits in the matrix.

IV. PROPERTIES OF THE SYSTEM

According to Eqs. (3)–(15), the properties of the proposed system are discussed by means of the simulation software MATLAB 2018a. Here, the four-input one-output Boolean function is selected as an example. After coding, the four input bits are converted to optical on-off keying signal with the bitrate $f = 10$ Gbit/s. The dispersion value of FBG is set as 1000 ps/nm. The modulation depth m_1 and m_2 are both chosen as 1. In the decoding process, the selection of threshold value can affect the system results. Here, the mean value of the time sequence x_3 is used as the threshold value x_{th}, which exhibits good results in the simulation.

Firstly, we focus our attention on the maximum number of available Boolean functions marked as *num*. Figure 4 reveals the relationship between the achievable number *num* and the loop iteration time *l*. In general, *num* keeps growing with the increasing of iteration time *l*. After accumulated nonlinear effects, eventually the input Boolean sequences can be transformed into any possible waveforms, sequentially resulting in various Boolean functions.

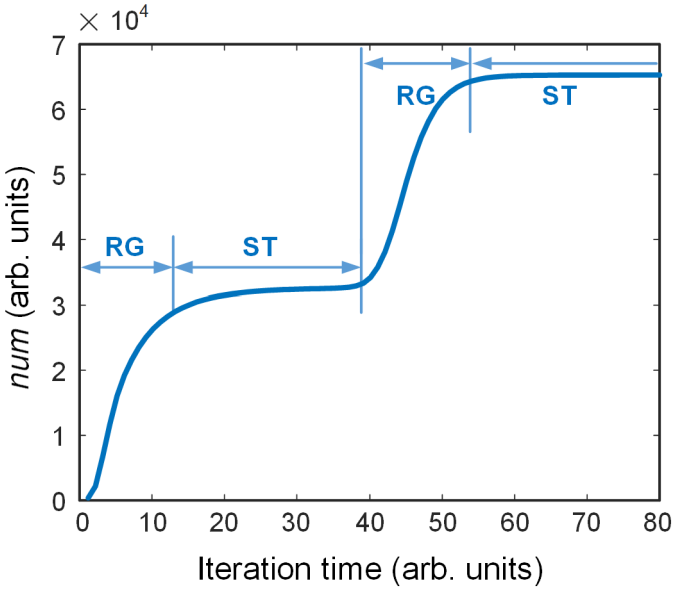

FIG. 4. Increase in the maximum number of available Boolean functions *num* with the iteration time *l*.

When *l* equals 75, *num* can reach its maximum theoretical value for a four-input one-output Boolean function. It means all possible Boolean functions can be realized in this optical system with adequate iterations. By setting a different control signal, the system can be reconfigured to a new Boolean function without changing its physical structure.

According to the increase rate of *num*, the growth curve exhibits two distinct characteristics in different periods, which are marked as steady transition (ST) region and rapid growing (RG) region. In the RG region, a slight increase of iteration time *l* can cause a marked rising of *num*. In contrast, to obtain reside functions in ST regions, a large number of iterations are spent. As can be seen, the whole curve consists of two RG regions and two ST regions, which appear in alternation. During the first RG period, 30 247 Boolean functions are acquired within 15 iterations. At the end of the first ST region ($l = 38$), about half the number of theoretical Boolean functions are produced, only adding an extra 2629 at the cost of 23 iterations.

The principle of this optical computing system is to utilize the ergodicity of a nonlinear dynamical system, which can transform a fixed initial state to any desired states. As stated in Fig. 1, the iteration circuit contains two transformations. The first one with the PM is used to mingle the iterating waveform and the control signal, thus making the generated Boolean functions controllable. The selection of Boolean functions is related to the differences between different control signals, which rely on the modulation index of PM m_1. The second one with the MZM performs the nonlinear transformation. For MZM, its nonlinear effect is determined by the modulation parameter m_2.

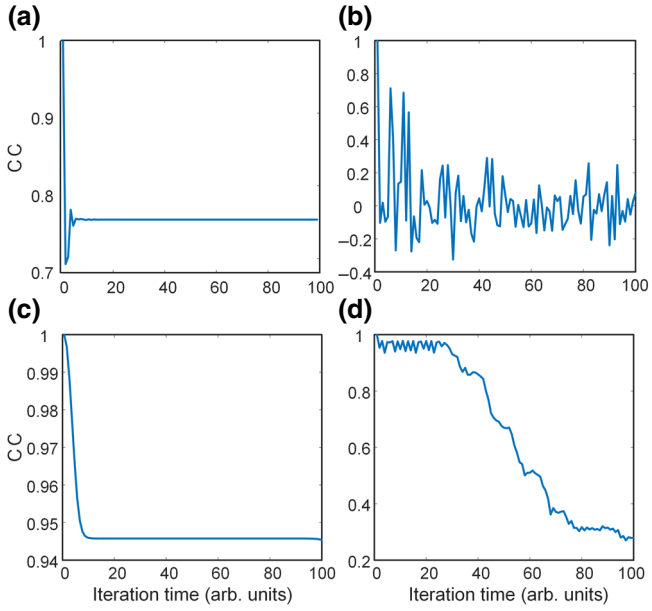

FIG. 5. Effect of two transforms on iterating waveform is studied, separately. The figures display the cross-correlation coefficients between the initial input and output waveforms after different iteration times. In (a), a small m_2 (= 0.2) is adopted, $m_1 = 2$. In (b)–(d), $m_1 = 0$, the values of m_2 are set as 2, 0.2, and 0.8, respectively.

Note that there is a long ST region between two RG regions in Fig. 4. In order to clarify the phenomenon, the effects of m_1 and m_2 are considered in detail. Firstly, the impacts of m_1 and m_2 on iterations of input waveform are investigated separately. In order to reflect the influence of optical transform on the input waveform, the cross-correlation coefficient (CC) is used to characterize the similarity between the input signal and output waveforms generated at different iteration loops. To discuss the effect introduced by m_1 individually, a small m_2 is adopted. Figure 5(a) plots the variation of CC at $m_1 = 2$ and $m_2 = 0.2$. After a short rapid oscillation, the CC comes into a nearly steady state. A large correlation value between the input and iterated output is maintained. In Fig. 5(b), the CC curve for $m_2 = 2$ is plotted, where the modulation index of PM m_1 and dispersion value of FBG d are set as 0. After several iterations, the CC decreases to a small value. Compared with m_1, m_2 plays a more important role in iterating the input waveform. The output result has a stronger dependence on the nonlinear effect of MZM.

When $m_2 = 2$, the nonlinear effect of MZM is relatively strong. The transform can make a big change on the input waveform, therefore the output of Boolean functions can be traversed quickly in a few loops. A further investigation of the influence of a small m_2 on the waveform is conducted. As shown in Figs. 5(c) and 5(d), the curves correspond to $m_2 = 0.2$ and 0.8, respectively. When $m_2 = 0.2$, the transformation approaches a linear expression, which causes little influence on the input waveform during the iteration process. For $m_2 = 0.8$, the waveform does have some minor variations after one iteration due to weak nonlinear effect. However, when the iteration repeats several tens of times, the CC can reach a small level. A significant change of the input waveform happens through repeating the nonlinear iteration. The cumulative nonlinear effect of continuous iterations can make a similar result as the strong nonlinear effect brings about. In other words, for a transform with a weak nonlinear effect, traversing all states can also be achieved at the cost of increasing iteration times.

Subsequently, the influences of m_1 and m_2 on the generated number of Boolean functions are studied. Figure 6(a) shows the tendency of the $num - l$ curve under different conditions of m_1, where m_2 is set as constant value 1. Seven curves discriminated by colors and markers correspond to m_1 taking 0.01, 0.05, 0.1, 0.5, 0.7, 1, and 1.2. As can be seen, a larger m_1 brings a larger *num*. For two different control signals, a large m_1 means a greater divergence, which is easier to obtain different Boolean functions. When $m_1 = 0.5$, the divergence reaches its maximum value, namely the half-wave voltage of PM. Hence, for $m_1 \geq 0.5$, the growth tends to be saturated, and the obtained number of Boolean functions remains nearly unchanged even if we further increase m_1. Nevertheless, all these curves can finally reach the theoretical value after adequate iterations.

As shown in Fig. 6(b), the variation of m_2 causes a considerable influence on the system characteristics. Here, m_1 is fixed as 1 and m_2 takes 0.1, 0.3, 0.5, 0.7, 1, 1.2, 1.5, 1.7, and 2. A smaller m_2 can restrict the total number of available Boolean functions. It is not capable of generating all possible functions when $m_2 < 0.5$. The second RG state disappears and is replaced by a longer ST region. When $m_2 \geq 0.5$, the second RG period appears. The appearance of the first ST region can be mainly attributed to the weak nonlinear effect of a single nonlinear iteration. The Boolean functions are discriminated by selecting different control signals. For two different control signals, nonlinear iterations can amplify their difference and result in two different outputs, which correspond to two different Boolean functions. The costs of iterating times are different for two similar control signals and two distinct signals. With limited iteration rounds, control signals with similar waveforms might generate an identical Boolean function. However, a single Boolean function can only be assigned to one control signal. In the first RG period, the generated Boolean functions are allocated to one of these similar control signals. With more and more Boolean functions appearing, the difficulty of generating new Boolean functions increases. In order to obtain reside Boolean functions, a drastic change of analog waveform is needed. However, under the weak nonlinear effect of a single iteration, a long iteration process is required to traverse the waveform to expected states, as demonstrated in Fig. 5(d). Therefore,

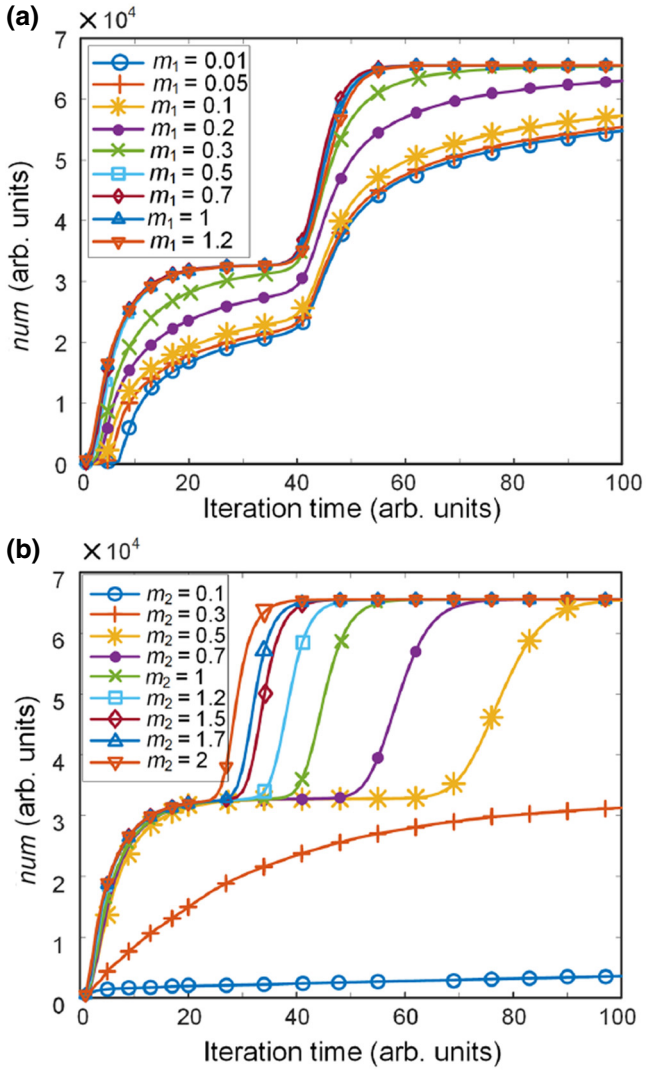

FIG. 6. Increase in the maximum number of available Boolean functions *num* with the iteration time l (a) under different phase modulation depth m_1 when $m_2 = 1$, (b) under different intensity modulation depth m_2 when $m_1 = 1$.

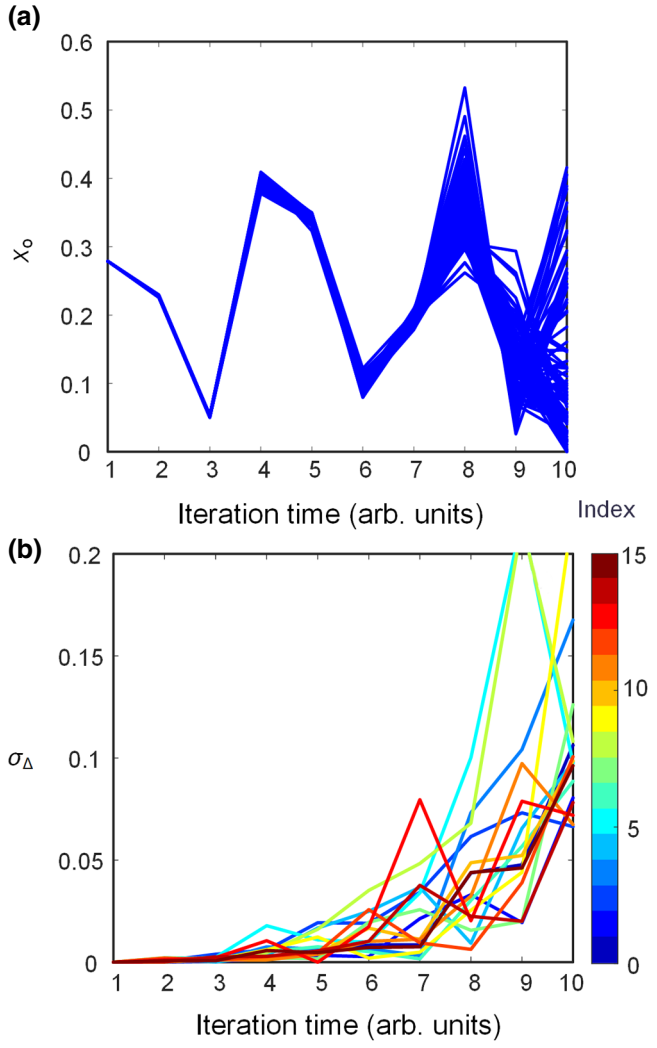

FIG. 7. (a) Divergence of sampling output x_o in 100 noisy trajectories; (b) the change of σ_Δ with iteration times l for all initial states.

the growth rate of available Boolean function during this period is slow, corresponding to the ST period. Through continuous iteration, the cumulative nonlinear effect is strong enough to make a big difference in the temporal waveform of output signal for similar control signals, and is thus capable of outputting another half of Boolean functions. With the enhancement of nonlinear effect of MZM, the duration of the first ST and second RG periods can be largely shortened. When $m_2 = 2$, the least iteration times in need is 59, and 75 times iteration is required for $m_2 = 1$.

V. THE INFLUENCE OF NOISE

In analog computation systems, noise can have a disastrous influence on their performance. With the increasing of cascade stages or iteration times, the accumulated contamination can even disable the normal operation. In Ref. [26], an improved scheme is proposed to reduce the effect of noise on the electrical Boolean function generator. In order to study the effect of noise, the Gaussian noise term is added to Eq. (9), which can be rewritten as

$$E_{\text{feed}}(t) = \sqrt{P_2}\cos\{m_2[x_2(t) + \text{noise}(t)] + \phi_{\text{bias}}\} \exp(j\omega_0 t + \phi_0) \quad (16)$$

noise(t) is an instantaneous term with zero mean and standard deviation σ. The value divergence of 100 trajectories is calculated with σ set as 0.001, which is identical to the value in Ref. [26]. Here, the initial state [0, 0, 1, 0] is selected as an example, which does not affect the main conclusions draw in this discussion.

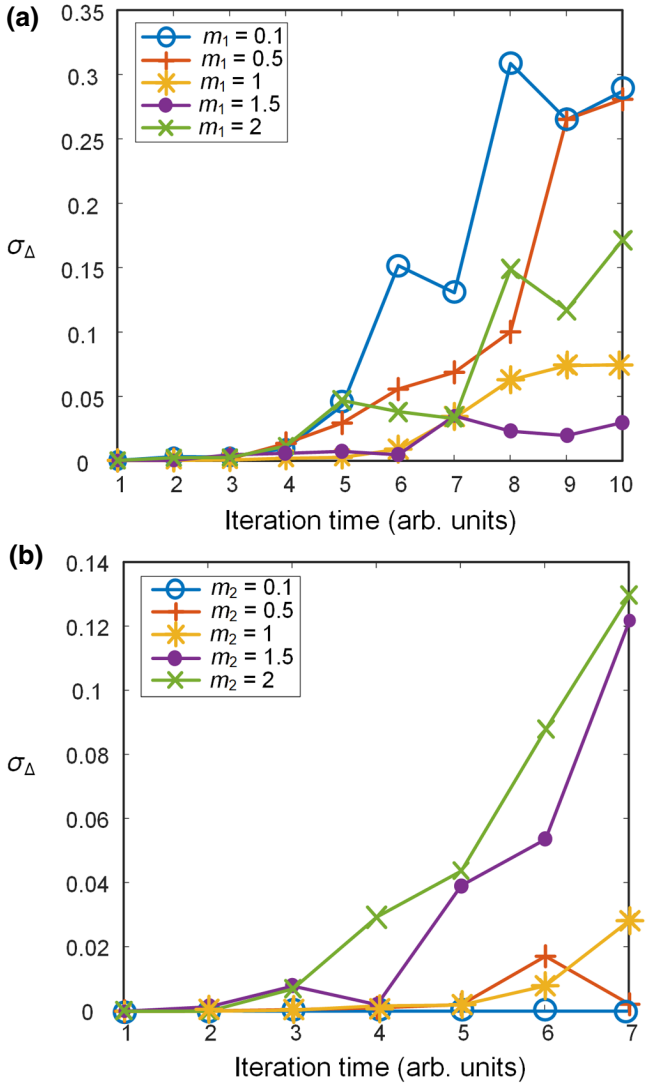

FIG. 8. Change of standard deviation σ_Δ using (a) different m_1 for $m_2 = 1$, and (b) different m_2 for $m_1 = 1$.

As shown in Fig. 7(a), when m_1 and m_2 are equal to 1, these trajectories begin to diverge dramatically at $l = 6$. To explain the noise effect further, a variable Δ is defined as the deviation of the noisy trajectory from the noiseless trajectory. The standard deviation σ_Δ of these trajectories is calculated to describe the fluctuation level of x_o caused by noise. Figure 7(b) shows the change of σ_Δ with the increase of iteration time l under all possible initial states, where [1, 1, 1, 1] is denoted as index 15 and [0, 0, 0, 0] is labeled as index 0. A stable iteration can be maintained before the sixth loop for all input states. As the iteration time increases, the accumulated noise plays an increasingly important role in the output waveform. With the participation of noise, it can be difficult to ensure the desired output after several nonlinear iterations.

As discussed above, the selection of m_1 and m_2 can affect the number of obtained Boolean function *num*. Larger m_1 and m_2 bring about a higher *num* in the first RG period. However, the variation of m_1 and m_2 could also influence the impact of noise on nonlinear iterations. Figures 8(a) and 8(b) show the change of standard deviationσ_Δ when using different m_1 and m_2. Because of the stronger nonlinear effect, a larger m_2 will aggravate the contamination of noise on the normal iteration. When $m_2 < 0.5$, the nonlinear iteration circuit can be more robust against the perturbations from noise. In other words, a larger iteration time is of permission under the same demand of low σ_Δ. However, this makes little sense on the increase of the number of achievable reliable Boolean functions due to their low growth rate of *num* in the first RG period. Considering the iteration time and growth rate simultaneously, in order to maximize the number of obtained Boolean function, range [0.5, 1] might be a good selection for m_2 under the corroding of noise.

Similar to m_2, a large m_1 can deteriorate the stability of output. Besides, a small m_1 can also result in a heavy deterioration on the system, as shown in Fig. 8(a). It might be attributed to the low signal-to-noise ratio of phase modulation since a small m_1 means a low modulation depth of signal. When $m_1 = 1$, corresponding to the green line in the figure, a better performance is exhibited against the influence of noise. When $m_1 = 1$ and $m_2 = 0.5$, 19 640 Boolean functions can be obtained after seven iterations with a relatively well robustness, where σ_Δ is below 0.01.

VI. CONCLUSION

In this paper, we propose a reconfigurable optical Boolean function generator. High-speed nonlinear calculation can be implemented utilizing the broadband property of optical components. The Boolean input modulates the driving current of the laser to generate optical on-off keying signal. This segment of waveform is used as the initial input of iteration, thus reducing the precise mapping procedure. Through the iteration circuit, a controllable nonlinear transform is performed on the input. The transform function is managed by the control signal. A different control signal provides a different nonlinear function, hence generating different output waveform. Through an average-detecting circuit, a different Boolean result can output. After numerous iterations, finally all functions are acquirable with no need of changing its physical configuration, which can exhibit a huge advantage in multifunctional computing and flexible configuration. A further simulation result reveals that a high nonlinear effect can enhance the speed to reach all possible functions, but also accelerate the degradation of noise. In the current scheme, lots of iterations are needed to implement all Boolean functions and the influence of accumulative noise is still heavy. By adjusting the values of nonlinear parameters m_1 and m_2, 19 640 reliable Boolean functions can be obtained in

seven iterations under the contamination of noise. The proposed scheme provides a solution to implement optical Boolean function computing and might be helpful for the exploration of following optical computation.

ACKNOWLEDGMENTS

This work is supported by The National Key R&D Program of China (Grant No. 2018YFB1801304); State Key Laboratory of Advanced Optical Communication Systems and Networks (LOCT) (Grant No. 2019GZKF7), National Natural Science Foundation of China (NSFC) (Grants No. 61675083, No. 61377073 and No. 61471179), Key Project of R&D Program of Hubei Province (Grant No. 2017AAA046).

[1] T. N. Theis and H.-S. P. Wong, The end of Moore's law: A new beginning for information technology, Comput. Sci. Eng. **19**, 41 (2017).

[2] J. M. Shalf and R. Leland, Computing beyond Moore's law, Computer **48**, 14 (2015).

[3] P. Ghelfi, F. Laghezza, F. Scotti, G. Serafino, A. Capria, S. Pinna, D. Onori, C. Porzi, M. Scaffardi, A. Malacarne *et al.*, A fully photonics-based coherent radar system, Nature **507**, 341 (2014).

[4] A. Khilo, S. J. Spector, M. E. Grein, A. H. Nejadmalayeri, C. W. Holzwarth, M. Y. Sander, M. S. Dahlem, M. Y. Peng, M. W. Geis, N. A. DiLello *et al.*, Photonic adc: Overcoming the bottleneck of electronic jitter, Opt. Express **20**, 4454 (2012).

[5] D. Brunner, M. C. Soriano, C. R. Mirasso, and I. Fischer, Parallel photonic information processing at gigabyte per second data rates using transient states, Nat. Commun. **4**, 1364 (2013).

[6] H. J. Caulfield and S. Dolev, Why future supercomputing requires optics, Nat. Photonics **4**, 261 (2010).

[7] D. A. Miller, Are optical transistors the logical next step? Nat. Photonics **4**, 3 (2010).

[8] J. Touch, A.-H. Badawy, and V. J. Sorger, Optical computing, Nanophotonics **6**, 503 (2017).

[9] K. Jain and G. Pratt, Jr., Optical transistor, Appl. Phys. Lett. **28**, 719 (1976).

[10] J. Touch, Y. Cao, M. Ziyadi, A. Almaiman, A. Mohajerin-Ariaei, and A. E. Willner, Digital optical processing of optical communications: Towards an optical turing machine, Nanophotonics **6**, 507 (2017).

[11] T. Houbavlis, K. Zoiros, A. Hatziefremidis, H. Avramopoulos, L. Occhi, G. Guekos, S. Hansmann, H. Burkhard, and R. Dall'Ara, 10 Gbit/s all-optical boolean XOR with SOA fibre Sagnac gate, Electron. Lett. **35**, 1650 (1999).

[12] K. E. Stubkjaer, Semiconductor optical amplifier-based all-optical gates for high-speed optical processing, IEEE J. Sel. Top. Quantum Electron. **6**, 1428 (2000).

[13] S. Ma, Z. Chen, H. Sun, and N. K. Dutta, High speed all optical logic gates based on quantum dot semiconductor optical amplifiers, Opt. Express **18**, 6417 (2010).

[14] X. Chen, L. Huo, Z. Zhao, L. Zhuang, and C. Lou, Reconfigurable all-optical logic gates using single semiconductor optical amplifier at 100-gb/s, IEEE Photonics Technol. Lett. **28**, 2463 (2016).

[15] D. Mendlovic and H. M. Ozaktas, Fractional fourier transforms and their optical implementation: I, JOSA A **10**, 1875 (1993).

[16] S. Liu, J. Xu, Y. Zhang, L. Chen, and C. Li, General optical implementations of fractional Fourier transforms, Opt. Lett. **20**, 1053 (1995).

[17] M. Cheng, L. Deng, H. Li, and D. Liu, Enhanced secure strategy for electro-optic chaotic systems with delayed dynamics by using fractional Fourier transformation, Opt. Express **22**, 5241 (2014).

[18] T. Zhongwei, Z. Nan, C. Ming, G. Taorong, R. Wenhua, T. Peilin, C. Yanling, and J. Shuisheng, in *2009 Asia Communications and Photonics Conference and Exhibition (ACP)* (IEEE, Shanghai, 2009), Vol. 2009, p. 1.

[19] C. Du, F. Cai, M. A. Zidan, W. Ma, S. H. Lee, and W. D. Lu, Reservoir computing using dynamic memristors for temporal information processing, Nat. Commun. **8**, 2204 (2017).

[20] A. Argyris, J. Bueno, and I. Fischer, Pam-4 transmission at 1550 nm using photonic reservoir computing post-processing, IEEE Access **7**, 37017 (2019).

[21] A. Argyris, J. Bueno, M. C. Soriano, and I. Fischer, in *The European Conference on Lasers and Electro-Optics* (Optical Society of America, Munich, 2017) p. CD_10_5.

[22] M. Sorokina, S. Sergeyev, and S. Turitsyn, in *2018 European Conference on Optical Communication (ECOC)* (IEEE, Rome, 2018), p. 1.

[23] D. Woods and T. J. Naughton, Optical computing: Photonic neural networks, Nat. Phys. **8**, 257 (2012).

[24] Y. Shen, N. C. Harris, S. Skirlo, M. Prabhu, T. Baehr-Jones, M. Hochberg, X. Sun, S. Zhao, H. Larochelle, D. Englund *et al.*, Deep learning with coherent nanophotonic circuits, Nat. Photonics **11**, 441 (2017).

[25] B. Kia, J. F. Lindner, and W. L. Ditto, A simple nonlinear circuit contains an infinite number of functions, IEEE Trans. Circuits Syst. II: Express Briefs **63**, 944 (2016).

[26] V. Kohar, B. Kia, J. F. Lindner, and W. L. Ditto, Implementing Boolean Functions in Hybrid Digital-Analog Systems, Phys. Rev. Appl. **7**, 044006 (2017).

[27] K. E. Callan, L. Illing, Z. Gao, D. J. Gauthier, and E. Schöll, Broadband Chaos Generated by an Optoelectronic Oscillator, Phys. Rev. Lett. **104**, 113901 (2010).

[28] M. Peil, M. Jacquot, Y. K. Chembo, L. Larger, and T. Erneux, Routes to chaos and multiple time scale dynamics in broadband bandpass nonlinear delay electro-optic oscillators, Phys. Rev. E. **79**, 026208 (2009).

[29] X. Gao, Enhancing ikeda time delay system by breaking the symmetry of sine nonlinearity, Complexity **2019**, 1 (2019).

[30] M. Mazur, N. K. Fontaine, R. Ryf, D. T. Neilson, H. Chen, G. Raybon, A. Adamiecki, S. Corteselli, and J. Schröder, in *2019 Optical Fiber Communications Conference and Exhibition (OFC)* (IEEE, San Diego, 2019), p. 1.

[31] M. Cheng, C. Luo, X. Jiang, L. Deng, M. Zhang, C. Ke, S. Fu, M. Tang, P. Shum, and D. Liu, An electrooptic chaotic

system based on a hybrid feedback loop, J. Lightwave Technol. **36**, 4259 (2018).

[32] M. Cheng, X. Jiang, C. Luo, Y. Fu, F. Luo, L. Deng, and D. Liu, Bistatic radar scheme based on the digital-analog hybrid chaos system, Opt. Express **26**, 22491 (2018).

[33] H. Chi, X. Zou, and J. Yao, Analytical models for phase-modulation-based microwave photonic systems with phase modulation to intensity modulation conversion using a dispersive device, J. Lightwave Technol. **27**, 511 (2009).

[34] J. J. Suárez-Vargas, B. A. Márquez, and J. A. González, Highly complex optical signal generation using electro-optical systems with non-linear, non-invertible transmission functions, Appl. Phys. Lett. **101**, 071115 (2012).